



UNIVERSITY OF LEEDS

This is a repository copy of *Optimised Vascular Network for Skin Tissue Engineering by Additive Manufacturing*.

White Rose Research Online URL for this paper:

<https://eprints.whiterose.ac.uk/174038/>

Version: Accepted Version

---

**Book Section:**

Ekinci, A, Han, X, Bibb, R et al. (1 more author) (2021) Optimised Vascular Network for Skin Tissue Engineering by Additive Manufacturing. In: Bidanda, B and Bártolo, PJ, (eds.) Virtual Prototyping & Bio Manufacturing in Medical Applications. Springer, Cham , pp. 1-20. ISBN 978-3-030-35879-2

[https://doi.org/10.1007/978-3-030-35880-8\\_1](https://doi.org/10.1007/978-3-030-35880-8_1)

---

© Springer Nature Switzerland AG 2021. This is an author produced version of an article published in Virtual Prototyping & Bio Manufacturing in Medical Applications. Uploaded in accordance with the publisher's self-archiving policy.

**Reuse**

Items deposited in White Rose Research Online are protected by copyright, with all rights reserved unless indicated otherwise. They may be downloaded and/or printed for private study, or other acts as permitted by national copyright laws. The publisher or other rights holders may allow further reproduction and re-use of the full text version. This is indicated by the licence information on the White Rose Research Online record for the item.

**Takedown**

If you consider content in White Rose Research Online to be in breach of UK law, please notify us by emailing [eprints@whiterose.ac.uk](mailto:eprints@whiterose.ac.uk) including the URL of the record and the reason for the withdrawal request.



[eprints@whiterose.ac.uk](mailto:eprints@whiterose.ac.uk)  
<https://eprints.whiterose.ac.uk/>

## **Optimised Vascular Network for Skin Tissue Engineering by Additive Manufacturing**

Alper Ekinici<sup>1</sup>, Xiaoxiao Han<sup>\*2</sup>, Richard Bibb<sup>3</sup>, Russell Harris<sup>4</sup>

<sup>1</sup> Wolfson School of Mechanical, Electrical and Manufacturing Engineering, Loughborough University, LE113TU, UK

<sup>2</sup>HNU College of Mechanical and Vehicle Engineering, Hunan University, Changsha, China

<sup>3</sup> Design School, Loughborough University, LE113TU, UK

<sup>4</sup> Mechanical Engineering, University of Leeds, LS2 9JT, UK

## **Abstract**

Artificial vascular vessels, including arteries, veins and capillaries, are being printed using additive manufacturing technologies. Additive manufacturing allows the manufacture of artificial blood vessels and their networks of any sophisticated geometry. This chapter demonstrates the essential and efficient methods to design and fabricate optimal vascular network for tissue engineering structures following the physiological conditions. Comprehensive physiological requirements in both micro- and macro- scales were considered in developing the optimisation design for artificial vascular networks. The optimised vascular vessel offers three advantages: (1) it provides the maximum nutrient supply; (2) it minimises the recirculation areas and (3) it allows the wall shear stress on the vessel in a healthy range. Two main design technologies are used in the chapter to achieve the design. They are computer graphics and computational fluid dynamics. The optimised design was then manufactured by the stereolithography process using materials that are biocompatible, elastic and surface bio-coatable. The stereolithography manufactured vascular vessels were embedded in the hydrogel seeded with cells afterward. The results of in vitro studies show that the optimised vascular network has the lowest cell death rate compared with a pure hydrogel scaffold and a hydrogel scaffold embedded within a single tube in day seven. The combination of the optimised micro- and macro- design, the material selection and the manufacturing methods completes a general guide for future artificial vascular vessel network developments.

**Keywords:** artificial vascular network, skin tissue engineering, additive manufacturing, stereolithography, design optimisation, computational fluid dynamics (CFD).

## 1 Introduction

Many clinical therapies utilise autologous and allografts to repair skin defects resulting from genetic disorders, acute trauma, chronic wounds or surgical interventions. Tissue engineering (TE) of skin is an emerging technology that offers many potential advantages in repairing skin defects over conventional autologous grafts [1]. It overcomes the shortage of donor organs and reduces the added cost and complications of tissue harvesting. Tissue-engineered skin can also be used as a skin equivalent for pharmaceutical or cosmetics testing, eliminating the need for animal testing [2]. A major issue in tissue engineering is that the artificial skin may not develop adequate vascularisation for long-term survival [3]. An artificial vascular system can be pre-embedded in a skin equivalent before it is implanted. The embedded network has three primary functions: (1) to supply nutrients and other soluble factors and to remove waste products from the surrounding cells, (2) to act as scaffolds for culturing vascular endothelial cells and (3) to develop small sprouting capillaries that can be connected with existing blood vessels, also known as angiogenesis [1], [4]–[6]. Nutrition supply in the human body is realised by a very complex blood vessel network. It consists of vessels in dimensions between several millimetres down to several micrometres in diameter. To mimic the system, flexible structuring processes are needed. Traditional manufacturing technologies, such as spinning, dip-coating or extrusion, can produce linear tubes with different inner-diameters [7]. However, it is not possible to generate branched vessels, with decreasing or increasing internal diameters to mimic the natural changes in blood vessel networks.

Additive manufacturing (AM) technologies have made it possible for the first time to manufacture artificial blood vessels and their networks of any sophisticated geometry and connections. With AM, three-dimensional (3D) objects can be produced from 3D computer-aided design (CAD) data by joining materials together using a layer-by-layer manner. There are many AM technologies classified as bioprinting systems, based on microvalve deposition, ink-jetting, material extrusion and stereolithography (SLA) techniques [8], [9]. SLA has advantages in 3D printing microvascular vessel networks due to (1) its high resolution, (2) its ability to produce flexible materials and (3) excellent process control. The use of these AM technologies will enable the generation and mimicking of complex blood vessel networks under controlled conditions. Currently, various research groups have successfully 3D printed and tested such vascular vessels [4], [10]–[13]. Wu et al., (2011) used transient inks to print a solid template within the substrate and then removed the ink to create microchannels. Hinton et al.,(2015) invented a freeform reversible embedding of suspended hydrogels method (called FRESH in their paper) to print hydrated materials that enable the printing of complex vascular architectures. However, in their work, vascular networks were printed with little understanding of the physiological demands. Therefore, general design guidance is missing. Design parameters such as branch levels, a branching point, branch angles, vessel diameter, the daughter vessel asymmetry ratio, wall shear stress (WSS) and recirculation areas should be considered carefully in the design of vascular vessels. Based on these parameters, this chapter presents guidance on the design optimisation of a vascular network manufactured by SLA for skin tissue engineering.

## 2 Design of Vascular Network

The main parameters considered in the design of a vascular network can be described in two categories: (1) the macroscale parameters and (2) the micro-scale parameters. The macro-scale parameters include branch levels and branching point locations, while the micro-scale parameters include branch angles, vessel diameters, the daughter vessel asymmetry ratio, the WSS and the recirculation areas. Their definition and illustration are shown in Figure 1.

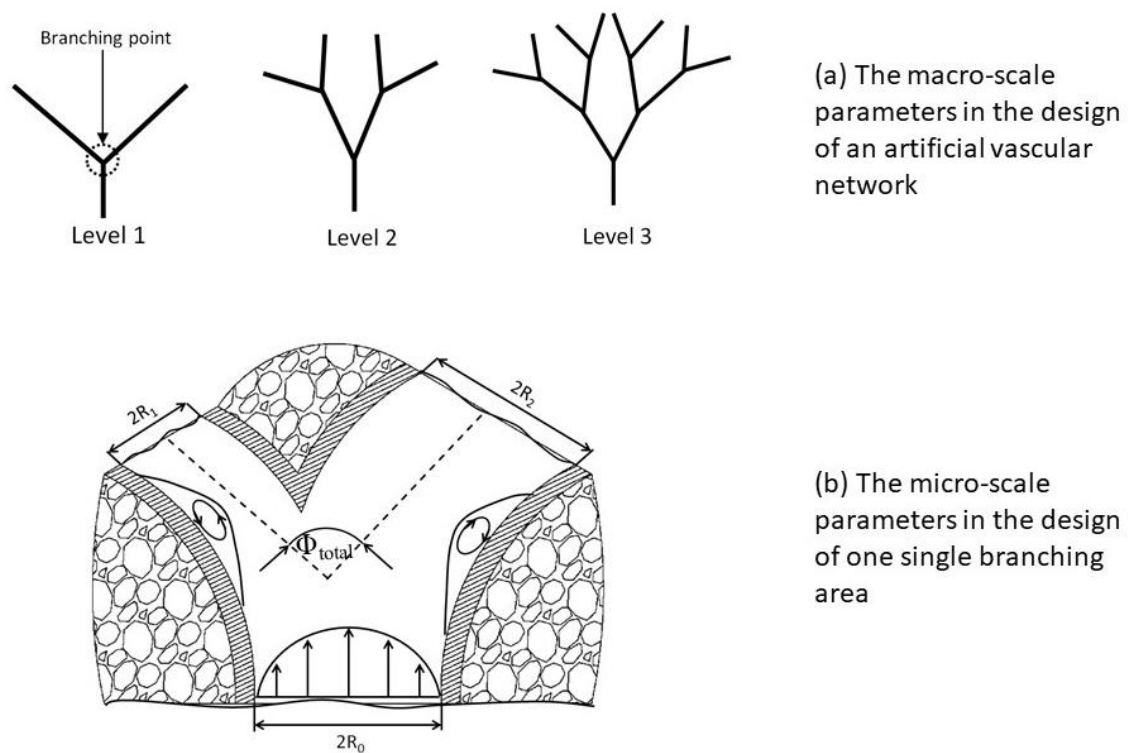


Figure 1: The macro-scale (a) and the micro-scale (b) parameter definitions [15]

In Figure 1 (a), branch levels and branching point are illustrated while Figure 1 (b) demonstrates parent diameter  $R_p$ , daughter diameters  $R_{d1}$  and  $R_{d2}$ , total branching angle, WSS and the recirculation areas.

## 2.1 Macro-Scale Design

The design of vascular networks is focused on bifurcations, because, in normal vasculature, around 98% of blood vessels bifurcate at each junction, while only 2% trifurcate [16], [17]. As the 3D structures can be formed by stacking 2D vascular systems, the locations of the branching points having different branching levels such as 2, 3, and 4 levels are evenly distributed on the skin patch, which can be illustrated in Figure 2 (a-c).

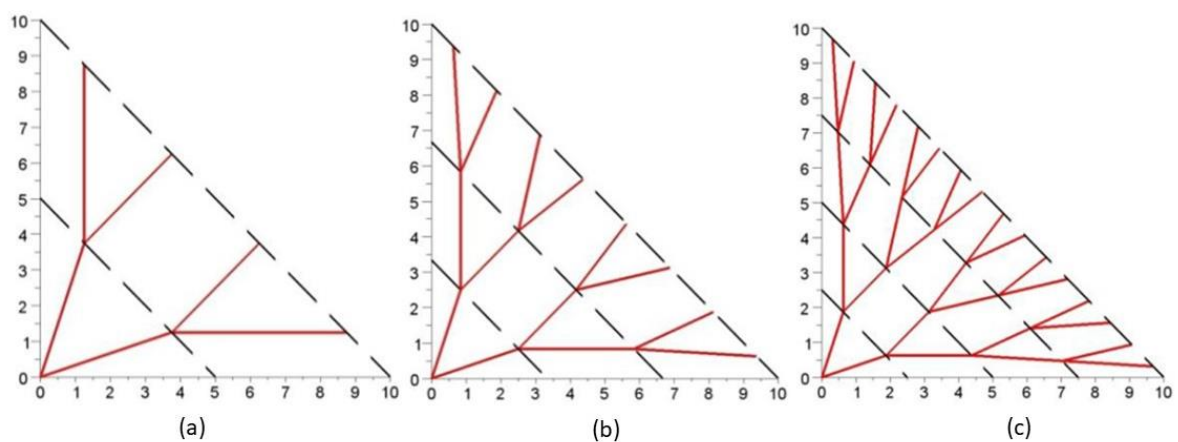


Figure 2: Distributed configuration of the vascular network with different branching levels:

(a) 2 levels, (b) 3 levels, (c) 4 levels [15]

The formula and calculation of different branching levels are given in details in [15]. Based on this calculation, the first configuration sketch of the vascular system is shown in Figure 3.

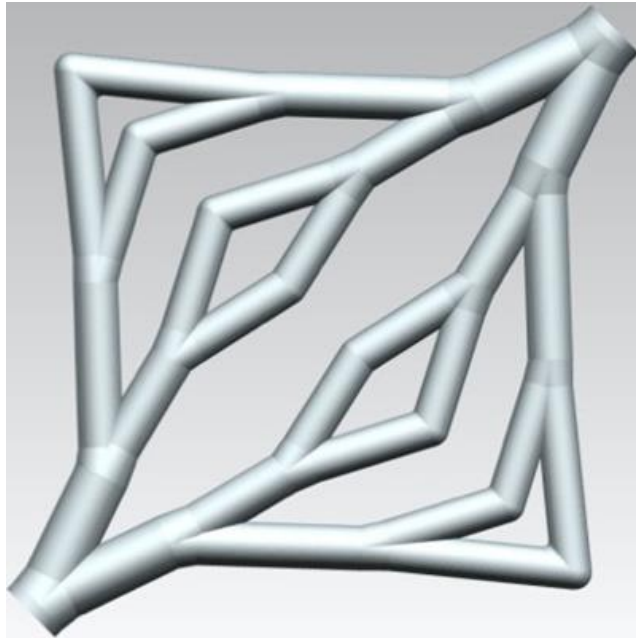


Figure 3: The first version of the vascular system [15]

It is shown that sharp junctions are used in all bifurcation points. These sharp apices at junctions of bifurcated vessels need to be avoided because they are considered risk factors for local mechanical weakness [18]. Rounding (increasing the radius) the apex at each junction can be one of the solutions. However, larger recirculation areas of blood are found in bifurcation vessels with rounded apices compared with sharp junctions [18]. Thus, a careful design of the bifurcation junctions is necessary. At the macro-scale, the main objective of the design is to maximise the nutrient supply and the waste exchange to surrounding tissues and cells; nevertheless, the local bifurcation design needs to ensure that the shear stress on the vessel wall is in the healthy range at the microscale.

## 2.2 Micro-Scale Design

The WSS is a critical haemodynamic indicator that affects endothelial cell development [17]–[20]. Many researchers have found that branching angles have a significant effect on WSS in the bifurcation of a branch vessel [21]–[24]. The maximum curvature of the junction

is the most important factor that influences WSS. High curvature also leads to stress concentration, which weakens the system mechanically [18], [19], [25], [26]. The volume (V) of the junction is another important factor in haemodynamics [27], [28]. A large volume leads to local recirculation of the blood [27], [28]. Another physiological requirement at the micro-scale is to ensure minimal recirculation areas where nutrient and oxygen may be trapped.

### 2.2.1 Branch Angle and Vessel Diameters

Design approaches to optimise a vascular network have been based on the minimisation of the sum of the energy required for pumping blood through the network and the energy required for the metabolic supply of the blood volume. To minimise the energy, Murray's law given in Equation 1 is applied [29], [30]:

$$R_p^3 = R_{d1}^3 + R_{d2}^3 \quad (1)$$

Using Murray's law, the radii of daughter vessels ( $R_{d1}$  and  $R_{d2}$ ) can be obtained based on the radius of their parent vessels ( $R_p$ ). It has been confirmed that most natural vascular systems follow Murray's law [31]. It is widely recognised that local geometries of a vascular bifurcation, such as bifurcation angles, junction curvatures and branching, are major features of the arterial system [20], [26].

The basic principle for a good junction design is therefore to ensure that the volume of the junction remains in a desired narrow range while limiting the maximum curvature. The exact range and limit depend on specific applications. Han et al. [32] developed a mathematical model using parameters such as bifurcation angles, and diameters of parent and daughter vessels. All the parameters in the model influence the junction volume V and the maximum



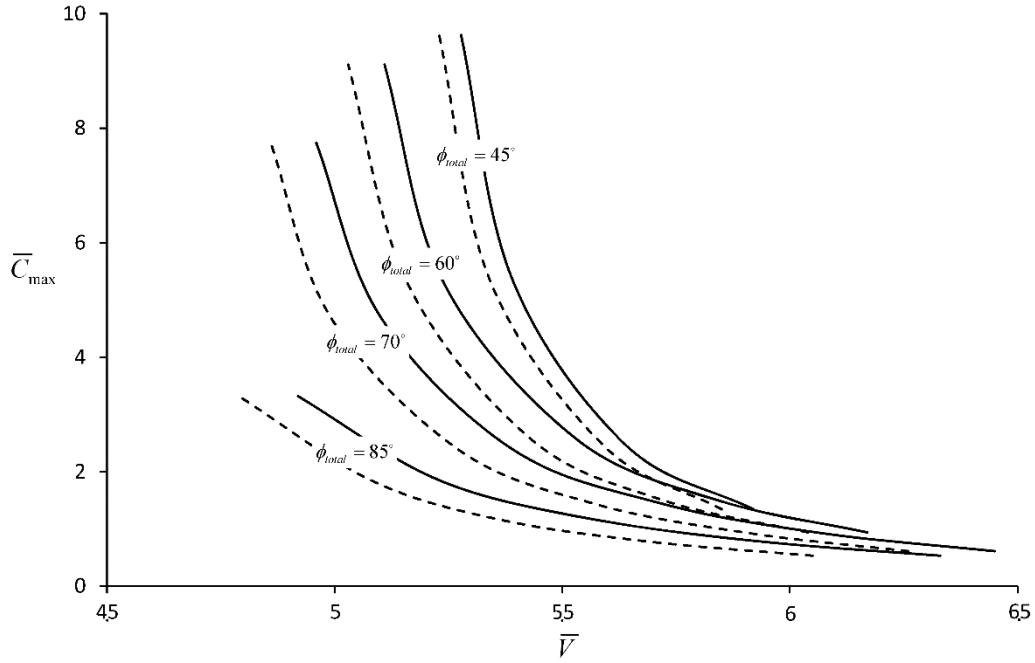


Figure 5:  $C_{\max} - V$  plots for different bifurcation angles:  $\varphi_{\text{total}} = 45^\circ$ ,  $\varphi_{\text{total}} = 60^\circ$ ,  $\varphi_{\text{total}} = 70^\circ$  and  $\varphi_{\text{total}} = 85^\circ$  [32]

For each bifurcation angle,  $\varphi_{\text{total}}$ , one dashed line and one solid line are plotted reflecting a band corresponding to different values of  $\alpha$  and  $\alpha$  is defined in Equation 2 as:

$$\alpha = \frac{\min(\varphi_1, \varphi_2)}{\max(\varphi_1, \varphi_2)} \quad (2)$$

The band is rather narrow showing the insensitivity to  $\alpha$ . Figure 5 can be used as a design guide to find the possible combinations of  $C_{\max}$  and  $V$ .

### 2.2.2 WSS and Recirculation Areas

Computational fluid dynamics (CFD) to study blood flow behaviour has to be based on accurate modelling of local vascular geometries [19], [20], [25], [27], [28]. Computer modelling of vascular bifurcation can be achieved in three ways: (1) skeleton based implicit surfaces [33]–[35], (2) blending objects obtained by canal surfaces [36], [37] and (3)

sweeping disks or spheres along curves [34], [38], [39]. Of all previous researches about modelling vascular structures, Cai et al. proposed a relatively simple method based on surface sweeping techniques [38], [39]. In medical imaging, every detail of the vascular geometry has to be captured accurately. In tissue engineering, on the other hand, one only needs to control some key factors when designing an artificial vascular network. It is therefore possible to select a simple method for the convenience of tissue engineering researchers.

Ensuring the smoothness of the junction and keeping a relatively small branch angle, as observed in the human body, is very important to avoid high WSS and recirculation. Vascular branches were constructed using the algorithm described in [32]. Figure 6 shows the midsections of the smooth branches with three different joining angles of  $45^\circ$ ,  $85^\circ$  and  $125^\circ$ .

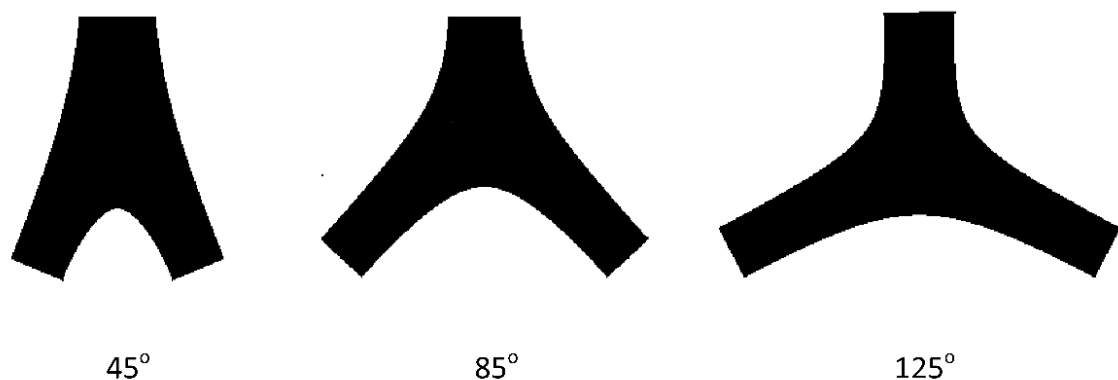


Figure 6: Mid-sections of the smooth branches with joining angles of  $45^\circ$ ,  $85^\circ$ , and  $125^\circ$  [40]

CFD simulations were carried out for haemodynamic analysis of different branch designs given in Table 1. The definition of parameters used in this table is fully explained in Han et al. [40].

Table 1: Value of controlled variables for different cases [40]

Cases	Parameters		
	Branch angle	$C_{max}$	V
1	125°	0.44	5.4
2	85°	1.43	5.4
3	45°	1.34	5.9
4	45°	3.02	5.56
5	45°	5.37	5.4
6	45°	7.5	5.3
7	45°	14	5.2

The purpose of the analysis is to compare the different designs in terms of the WSS and flow behaviour. CFD simulations were performed for cases 1, 2 and 5. In all cases two flows merge from the daughter vessels into the branch leading to a volume expansion. Using the same branching volume for all the three cases, the effect of branch geometry such as the branching angles can be analysed. The negative velocity observed in all the cases indicates backflow. In Figure 7, it can be observed that the backflow induces recirculation in the branching area. Two vortices can be seen in the branching area although its magnitude is small comparing with the surrounding velocity field. A region with low-velocity vortices is known as a flow recirculation area.

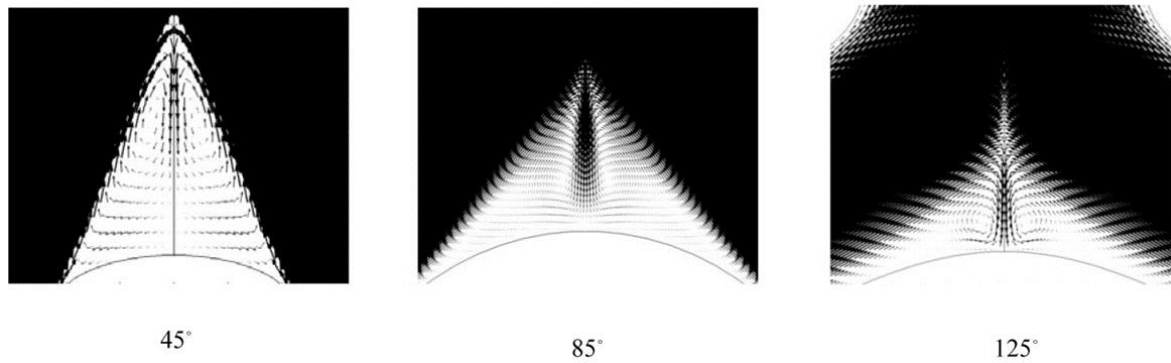


Figure 7: Recirculation area for branching angles 45° (case 5), 85° (case 2) and 125° (case 1)

[40]

Nutrients for arteries or waste for veins in the blood flow can be trapped in such area. Therefore, it is important to understand how the recirculation area of a rounded junction affects the flow velocity profile and the wall WSS downstream. In Figure 7, the ratios of recirculation area over the whole branch are (1) 45°: 26.4%, (2) 85°: 24.9% and (3) 125°: 21.8%. Junction with 45° branch angle has the largest recirculation area, while junction with 125° branch angle has the smallest recirculation area.

WSS is one of the most significant haemodynamic factors that relate to blood vessel development and cardiovascular diseases [19], [25], [26]. In healthy cerebral arteries, the WSS ranges from 1 to 7 Pa [41]. WSS higher than 7 Pa can damage the endothelial cells during vascular remodelling while WSS lower than 1 Pa can lead to the formation of plaque due to insufficient mechanical stimulation on endothelial cells [41]. WSS distributions for different smoothed cases and their sharp counterparts are shown in Figure 8.

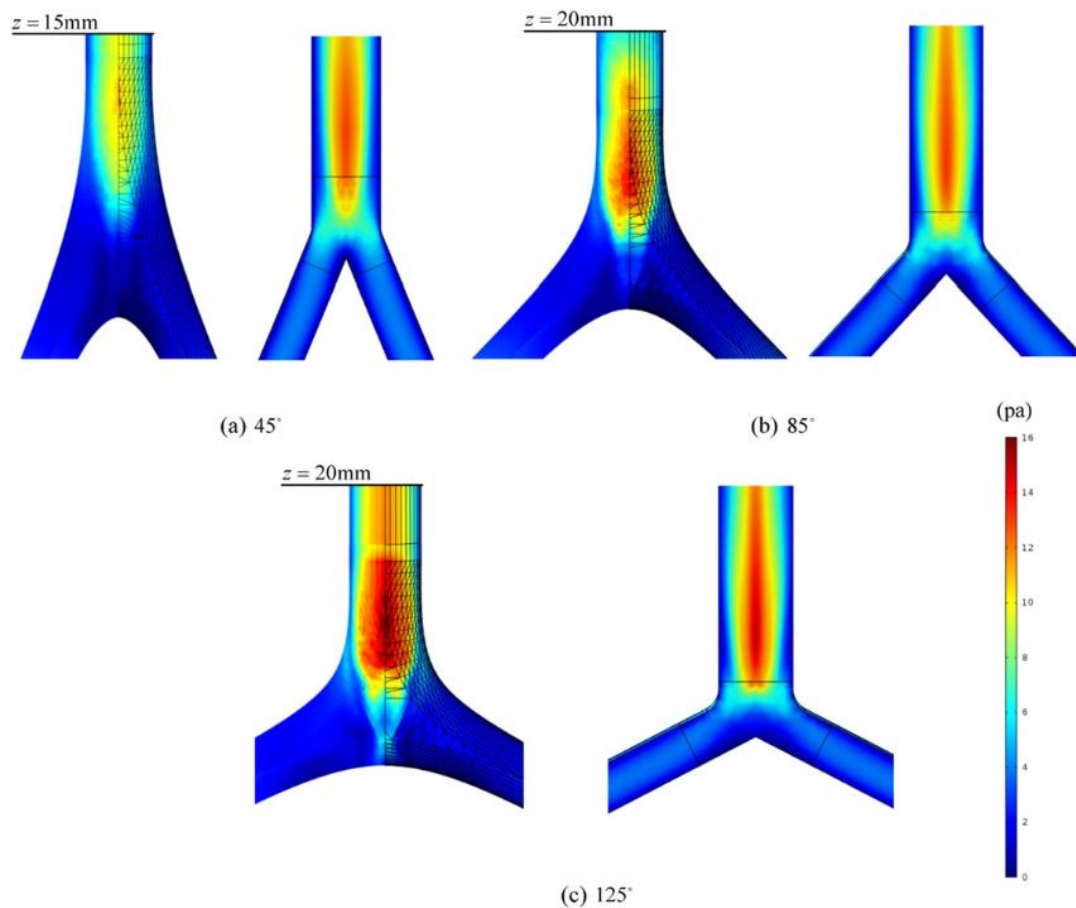


Figure 8: Wall shear stress distribution for branching angles (a) 45°, (b) 85° and (c) 125° for the smoothed model (left) and sharp model (right) [40]

In the junction, the WSS can be many times higher than that in the straight vessel. WSS in the smoothed junction has a different distribution compared with those in the sharp junctions. High WSS (12 Pa) is found on the sharp junction compared to the rounded one (10 Pa) as shown in Figure 8 (a). The area of low WSS in the smoothed junction is larger than that in the sharp one due to recirculation. Figure 8 (a) shows that at  $z = 15\text{ mm}$ , the WSS distribution is more uniform with a low average value of 4 Pa in comparison with 5 Pa in a sharp junction. In Figure 8 (b), similar values of maximum WSS can be observed for both models ( $\sim 14\text{ Pa}$ ). In the smoothed model, the distribution of WSS is more intense at the beginning of the downstream flow, but a more uniform distribution of low values is found at

$z = 20$  mm in comparison with the sharp model. It is found in Fig. 1.8c that the recirculation area has a similar but weak influence on the WSS distribution in a rounded junction in comparison to the sharp junction. A correlation between the WSS reduction and the bifurcation angle is shown in Figure 9.

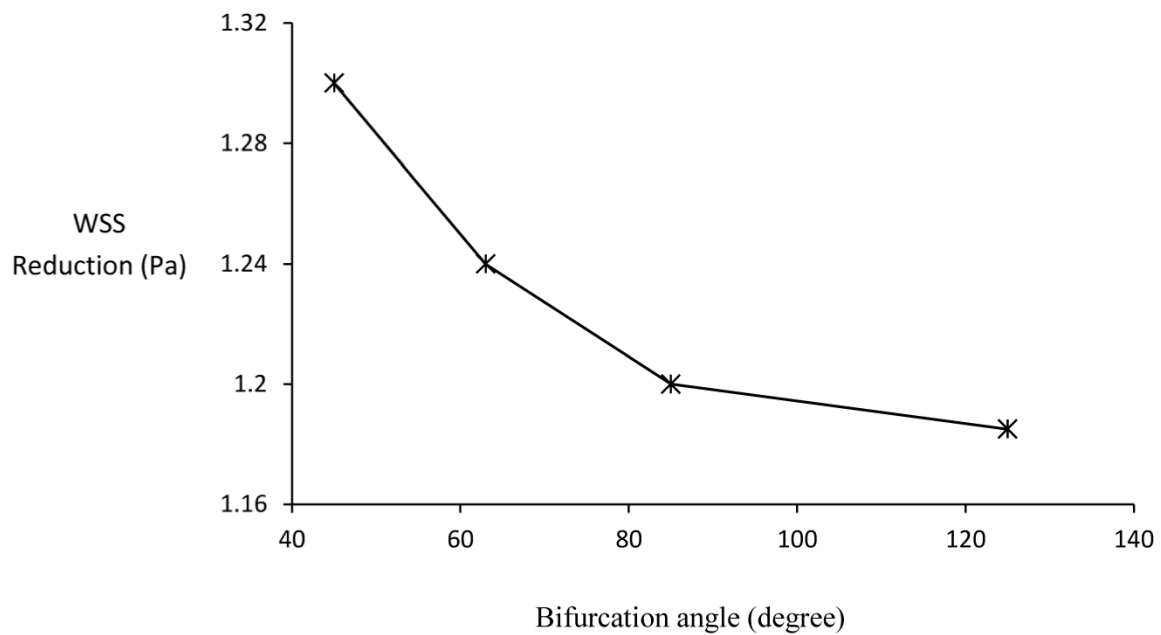


Figure 9: WSS reduction at  $z = 0.15$  (m) using parametric model compared with sharp bifurcations versus bifurcation angle [40]

From Figure 9, it is seen that junctions with larger bifurcation angle result in a smaller WSS reduction. With further increase in the bifurcation angle, the WSS reduction decreases more slowly. This indicates that the smoothed design has less effect on WSS reduction downstream for bifurcations with larger angles. In the parametric design model of a branch junction,  $C_{max}$  and its corresponding  $V$  are the most important geometric parameters. A larger  $C_{max}$  leads to a smaller  $V$ , thus a smaller branching area. Further increasing  $C_{max}$ , however, has a limited effect on the branching area as  $V$  will decrease more slowly. In this

section, CFD simulations are presented for smoothed junctions with different  $C_{max}$  for a branching angle of  $45^\circ$  (cases 3–7).

### 2.2.3 Daughter Vessel Asymmetry Ratio

According to [42], the WSS in a vascular bifurcation is related to two local parameters. They are  $R^+$ , the asymmetry ratio and the total bifurcation is shown in Figure 1 (b) and  $R^+$  is calculated using Equation 3:

$$R^+ = R_{d1}/R_{d2} \quad (3)$$

Khamassi et al. [42] established a CFD simulation to analyse how  $\alpha$  and  $R^+$  effect the minimal WSS at bifurcation junctions. They also generated a diagram to explain their correlations. This diagram is used as a guide for the selection of bifurcation angles shown in Figure 10.

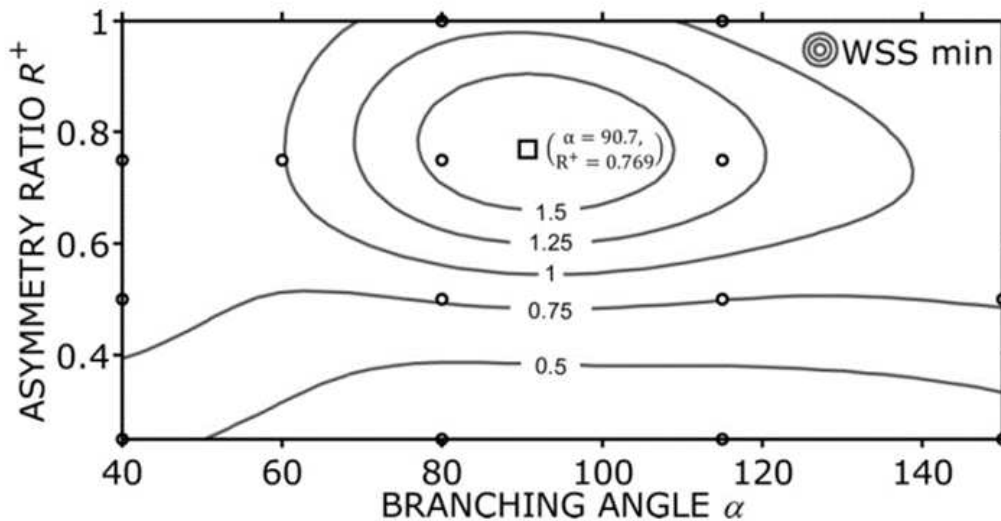


Figure 10: WSS as a function of the bifurcation geometry [15]

In Figure 10, the circles represent the founding WSS using different combinations of  $R^+$  and  $\alpha$ . The contour lines in Figure 10 demonstrate the interpolated WSS values based on the founding values. A distinct optimum appears when  $R^+$  is shown as a square in Figure 10. This

diagram suggests that the branch angle and the asymmetry are the major geometry parameters of physiological bifurcations. The selection of bifurcation angle and the asymmetry should be in the range of the contour lines to lead to proper function: the bifurcation angle ranges from  $60^\circ$  to  $140^\circ$ , while the asymmetry ratio ranged from 0.6 to 1.

In the first version of the vascular system, bifurcation angles and the asymmetry were checked, and it was found that two bifurcation angles were out of the range. An algorithm was then developed to fix the problem [15]. By updating this algorithm, the bifurcation points with sharp apices are rounded as can be seen in Figure 11.

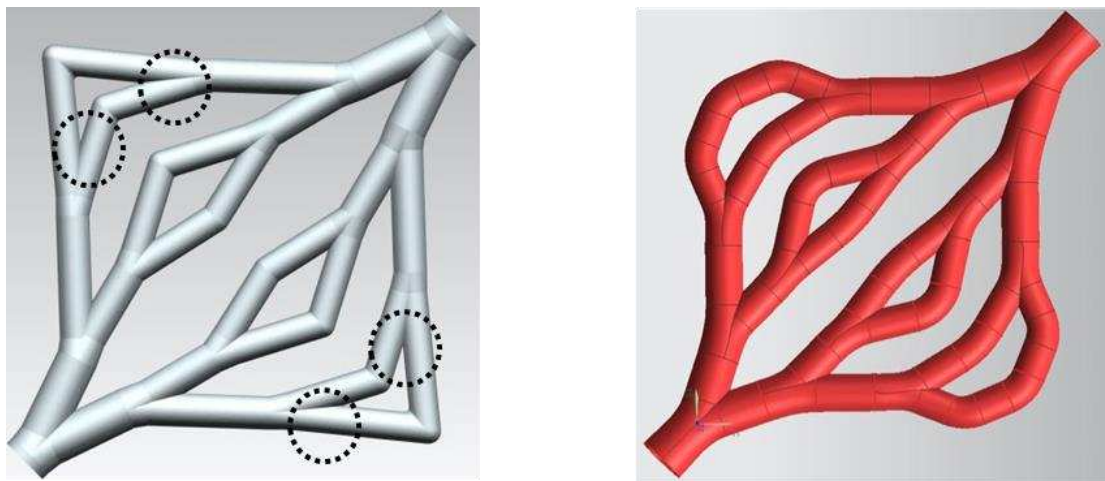


Figure 11: The new version of the vascular system [15]

To optimise a vascular network embedded in the skin patch to supply tissues and cells with nutrients and oxygen, exchange waste and to support angiogenesis, design criteria are considered in both macro-scale and micro-scale. It can be described as four criteria, which are as follows:

- to maximise the nutrient supply and waste exchange
- to minimise the resistance to blood flow
- to ensure the shear stress on the vessel wall is in the healthy range

- to avoid the blood recirculation.

### **3 The Application: Optimised Vascular Network Design for Skin Tissue Engineering**

Selecting the material and manufacturing technologies are important while designing a vascular network for skin tissue engineering using SLA. The material selected for manufacturing of a vascular network needs to have appropriate viscosity and polymerisation characteristics to allow it to be 3D printed successfully. Additionally, it also needs to have vessel-like properties, such as appropriate elasticity, biocompatibility and surface readiness for bio-coatability. The well-proven AM process SLA makes it possible to manufacture complex geometries such as a vascular network.

#### **3.1 Additive Manufacturing Technologies for Biomanufacturing**

SLA was developed in 1980s and was one of the first commercial AM processes [43], [44]. Conventional SLA machines have vertical resolutions in the range of 150  $\mu\text{m}$ . Further developments known as “micro SLA” can create geometries with high complexity [45] and with resolutions below 150  $\mu\text{m}$  in all three spatial directions. Layer heights of less than 10  $\mu\text{m}$  allow the replication of capillaries that are essential for the metabolism in the tissue. Alternative AM methods are not able to produce such high-resolution structures [10], [46]. The high resolution of AM cell scaffolds or membranes enables targeted cell alignment, cell growth and cell interaction [46], [47]. The SLA process relies on a photo-polymerisation process and suitable resins consist of monomers and photoinitiators (PI) that are typically toxic. Consequently, for biomedical applications, it is paramount to guarantee that the PI degrades completely during the polymerisation process. This challenge can only be overcome by interdisciplinary process improvement, including material, SLA process and

environmental conditions since in state-of-the-art implementations a typical degree of polymerisation is between 40 and 70% resulting in a considerable amount of remaining PI [48]. A promising approach to guarantee complete polymerisation and to prevent the formation of unwanted compounds uses inert atmosphere. Only in the absence of oxygen, it is possible to achieve complete crosslinking and full disappearance of cytotoxic PI and monomers.

### 3.2 Materials and Methods

The material chosen for the application consisted of three monomers plus a photoinitiator. The formulations are BPA-ethoxylated-diacrylate, lauryl acrylate and isobornyl acrylate (BLI). Three types of photoinitiator were tested to select the most appropriate one that has the lowest cytotoxicity. They are Irgacure<sup>®</sup> 184, Irgacure<sup>®</sup> 2959 and Irgacure<sup>®</sup> 369. BLI samples with three photoinitiators were investigated by the two methods WST-1 assay (three replicates of each kind of a material; characteristic of the sample: diameter: 14 mm, height: 1–2 mm, weight: 200 mg) and live/dead assay (characteristic of the sample: diameter: 14 mm, height: 2–3 mm, weight: 300 mg). All samples were disinfected in 70% ethanol for 30 min (meanwhile the samples swelled), washed two times for 30 min with PBS and equilibrated in cell culture medium.

In the WST-1 assay, eluates from different specimens were tested for cytotoxic components. The specimens were eluted by incubation in complete cell culture medium for 24 h and following periods at 37°C. According to ISO norm 10993-5 a volume of 1 mL medium was applied per 0.2 g material. Eluate samples were taken after 1, 2, 3, 6, 7, 8, 9, 10, 13, 15, 17, 21 and 24 days and the medium was completely renewed. The elution period day 0–1, 1–2, 2–3, 6–7, 10–13 and 21–24 was finally tested. For this 3T3 cells have been pre-cultured for 1

day in a 96 well tissue culture plate inoculated with care with about 8,000 cells per well. Then the medium was changed against the eluate samples (four replicates from each eluate sample resulting in 12 replicates representing the same material sample) and cells were incubated with the eluates for 24 h under cell culture conditions at 37°C in a 5% CO<sub>2</sub> atmosphere. The negative control (representing no cytotoxic influence) received pure cell culture medium, whereas the positive control (representing highest level of cytotoxicity and complete inhibition of dehydrogenase activities) was obtained from wells without cells containing only culture medium. Eluate samples and controls were changed after 24 h against medium with WST-1<sup>®</sup> reagent but without phenol red and cultured for about 20 min to 1 h. Formation of coloured formazan was measured by the optical density at 450 nm. The development of dye intensity was kept under control to measure at a time point, when the optical density of the negative control was between 0.2 and 0.6.

### 3.3 *In Vitro* Testing

Human adipose-derived stem cells (hASCs) and pericytes were isolated from human tissue derived from patients that underwent regular surgical treatment and signed an informed content at the BG University Hospital Bergmannsheil in Bochum, Germany. The hASCs were cultured in DMEM-HAMS-F12, and the pericytes were cultured in a pericytes-growth-medium (PGM, PromoCell).

In the context of the study as a scaffold methacrylated gelatine (5%; IGB) was used [4]. Using methacrylated gelatine and a photoinitiator (LAP; INN) a stable hydrogel was created. Within this hydrogel, three diverse species of cells were spread: 600,000 HUVECS, 600,000 hASCs and 60,000 pericytes. In the hydrogel three different shapes of tubes were created:

(1) a stainless steel moulded tube, (2) a single tube 3D printed by SLA using BLI with Irgacure® 184 and (3) a branched network 3D printed by SLA using BLI with Irgacure® 184.

The bioreactor system developed in [22] was driven by a pump-sleeve-system to deliver medium (620  $\mu\text{l}/\text{min}$ ) to the hydrogels. The pump was connected to a nutrient bottle and the hydrogel containing chamber (see Figure 12). To run the bioreactor system a medium mixture was performed in the same ratio as the corresponding cells were distributed. The hydrogels were cultured at 37°C and 5% CO<sub>2</sub> for 7 days.

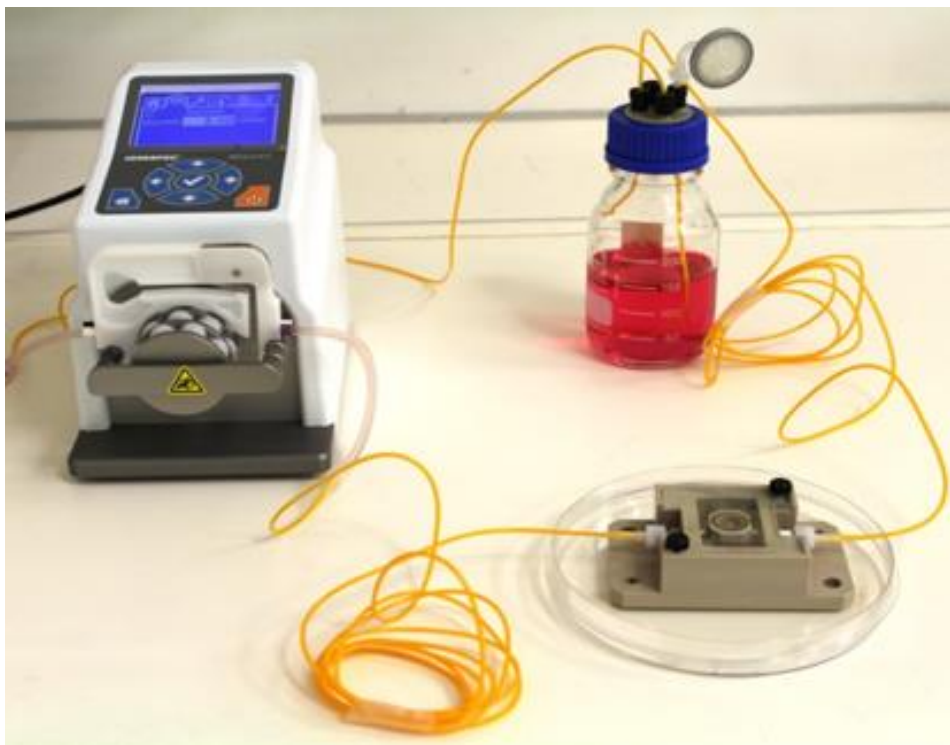


Figure 12: The bioreactor system used for the tube supported tissue culture [15]

After 7 days a live/dead assay was performed staining the hASCs with calcein (green) and Propidiumiodid (red).

## 4 RESULTS and DISCUSSION

### 4.1 Cytotoxicity Testing for Photoinitiators

Firstly, in the live/dead assay, to evaluate the cytotoxic effect observable in case of direct contact of the cells to the material, the percentage of dead cells was determined by manually counting live and dead cells from fluorescence micrographs. Below 5% dead cells (during longer culture below 10%) was considered to be not cytotoxic since this can be observed in control cultures too. Low cytotoxicity is assumed from 5% to 20% dead cells, moderate cytotoxicity is from 20% to 50%, and high cytotoxicity is above 50%. Already the viability staining revealed the high cytotoxicity of BLI with Irgacure® 2959, where no viable cells could be at BLI with Irgacure® 184 and at BLI with Irgacure® 369 developed higher cell densities from about 135–225 to 360–625 cells/mm<sup>2</sup> during culture time and had less than 10% dead cells (Table 2).

Table 2: Levels of cytotoxicity determined by live/dead staining [15]

<b>Material</b>	Control (glass)	BLI with Irgacure® 184	BLI with Irgacure® 2959	BLI with Irgacure® 369
<b>Day 1</b>	No cytotoxicity	No cytotoxicity	High cytotoxicity	No cytotoxicity
<b>Day 4</b>	No cytotoxicity	Low cytotoxicity; increased number of cells from day 1 to day 4	High cytotoxicity	Low cytotoxicity; increased number of cells from day 1 to day 4
<b>Day 14</b>	No cytotoxicity	Low cytotoxicity	High cytotoxicity	Low cytotoxicity

## 4.2 The Printed Vascular Network

The SLA process was developed in this work to produce the vascular network. It consists of a polymer bath, a laser and a scanner system with an F-theta lens ( $f=100\text{mm}$ ) for fast beam deflection in x-y-direction. The polymer bath was positioned on a platform connected to a piezo-axis to allow positioning in the z-direction. For process development, different photo resins in combination with a photoinitiator 355 nm were investigated. Detailed SLA setting is shown in Figure 13.

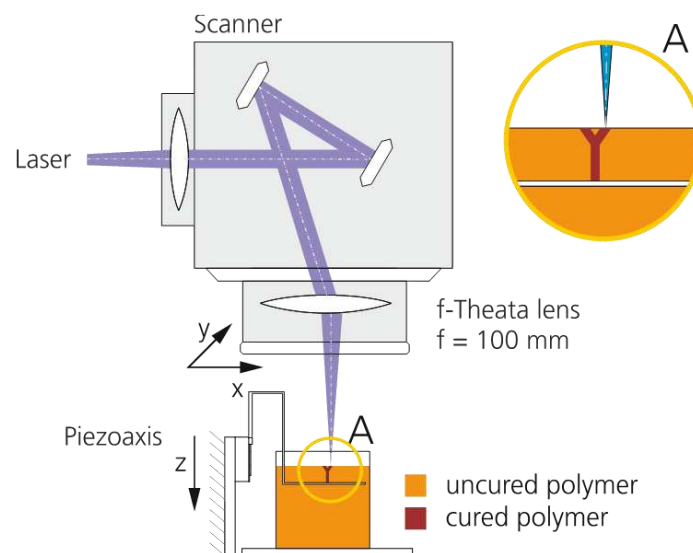


Figure 13: SLA process setups [15]

To define a reliable process regime, PI concentration (0.5 wt% and 1 wt%), scan speed (5–600mm/s), layer thickness (30 $\mu\text{m}$ , 100 $\mu\text{m}$ , 150 $\mu\text{m}$ ) and the distance between two lines were varied. Firstly, photo resin 3D-03H-87, Marabu with 1wt% PI was used in printing to get the best set of parameters, which were 15 kHz, power: 10.1 mW, scan speed: 80 mm/s, line distance 30 $\mu\text{m}$  and a layer thickness: 800 $\mu\text{m}$ . Non-crosslinked photo resin was washed away with ethanol (70%). A branched vessel system was also printed from this material using the above parameters. It is showed that by using the SLA technique, the designed branched

blood vessel network could be constructed. The structure of the printed vascular network using BLI with Irgacure® 184 with pores is shown in Figure 14.

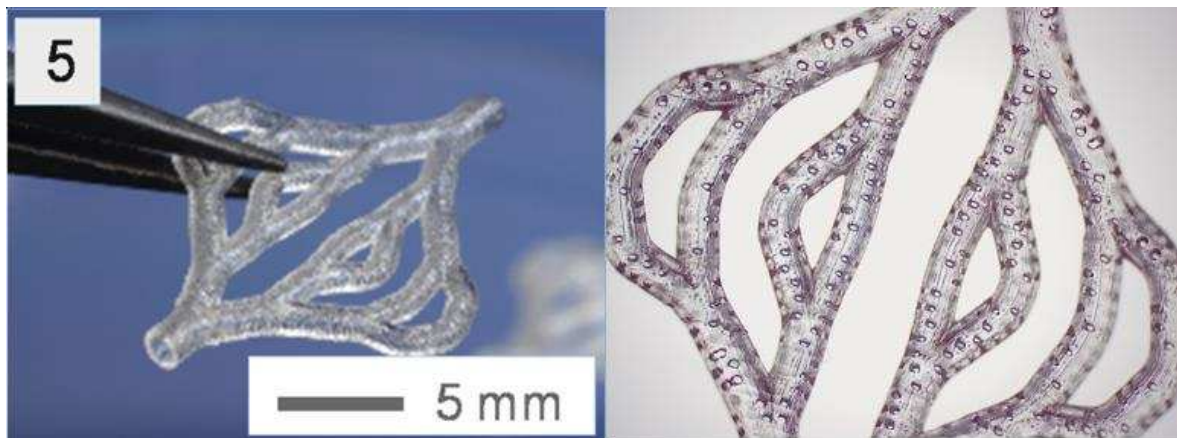


Figure 14: The structures of the printed branched vessel network using BLI with Irgacure® 184 with pores [15]

The printing accuracy of angles and pores was tested by flow test with dye solution. It demonstrated that all pores were open. In the first experiments it was observed that branching angles show irregularities due to pores or problems from data slicing.

#### 4.3 *In Vitro* Testing

hASCs were evaluated regarding their viability using a live/dead assay for 7 days of culture. Results of cell viability are shown in Figure 15.

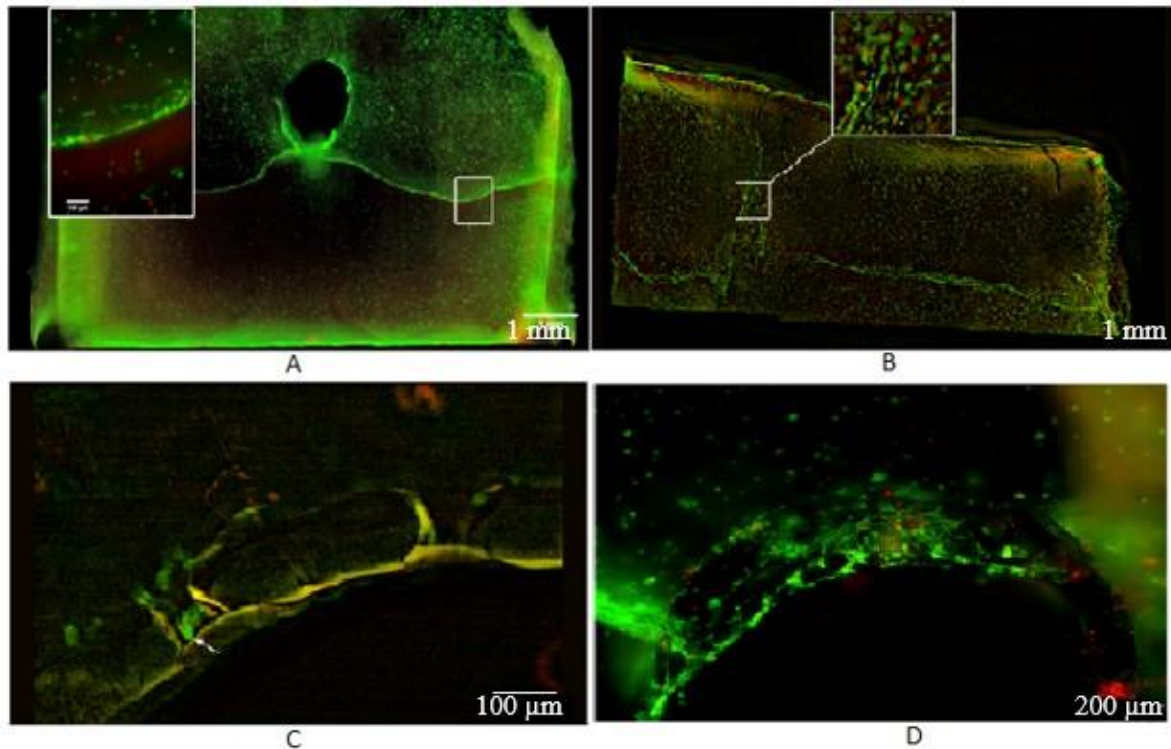


Figure 15: Cell vitality within a 1 x 1 cm hydrogel supported via (a) a stainless steel moulded central tube; (b,c) a branched BLI with Irgacure® 184 tube containing pores (d) single central SLA-formed BLI with Irgacure® 184 tube containing pores [15]

Figure 15 illustrates the cell vitality within a 1 x 1 cm hydrogel supported via a stainless steel moulded central tube (Figure 15 (a)), an SLA-formed branched PA tube containing pores (Figure 15 (b-c)) and a single central SLA-formed PA tube containing pores (Figure 15 (d)). By comparing Figure 15 (a-b), it is demonstrated that the ability of a branched tube can support the whole volume more appropriately compared with the central steel tube. Additionally, it is also shown that the surrounding cells get in contact to parts of the materials, infiltrating the pores (in Figure 15 (c)) and form more complex structures within the hydrogel (in Figure 15 (d)). Figure 16 gives a preliminary comparison of dead cell rate with different embedded tubes. It can be seen from this picture that after 7 days, cell death rate in the branched

vessel is the lowest (27%) compared with the pure hydrogel (35%) and hydrogel with a single tube (55%).

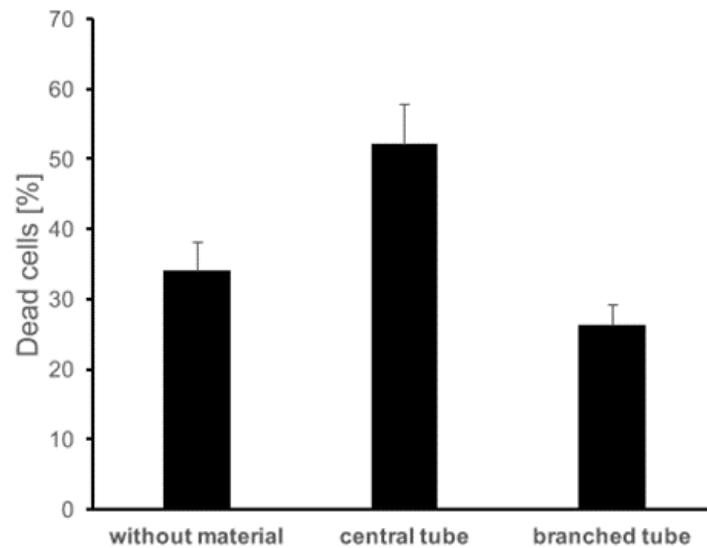


Figure 16: The dead cell rate (%) after seven days with no embedded tube, single tube and branched tube (sample size for each is 3) [15]

The pure hydrogel used as a scaffold in this work has proven to be non-toxic and has a good biocompatibility. This can also be seen in Figure 16 that the pure hydrogel scaffold has less than 50% percent cell death rate after 7 days. The curable resin made of BLI with Irgacure® 184 was proven to be biocompatible and cytocompatible.

## 5 Conclusion

In this chapter, an optimised vascular network was developed using a set of comprehensive design rules. These design rules considered the physiological requirements in both macro- and micro-scales. The vascular network is optimised not only to provide the maximum nutrient supply with minimal complexity but also to minimise recirculation areas and to keep WSS in a healthy range. For an application study, a suitable photo-curable resin which

is elastic, biocompatible and bio-coatable with photoinitiators was selected. Among three resins, the results show that BLI with Irgacure® 184 has the lowest cytotoxicity and it was used with an SLA equipment to 3D print the design. SLA enables the manufacture of complex three-dimensional bifurcated vascular networks with controllable geometries. The results of the 3D printed design in preliminary *in vitro* studies showed that the branched resin vascular network had the lowest cell death rate. The design and manufacturing route for skin tissue engineering proved in this chapter can be used as a guide to design and manufacture an optimised vascular network.

## 6 References

- [1] R. A. Kamel, J. F. Ong, E. Eriksson, J. P. E. Junker, and E. J. Caterson, "Tissue engineering of skin," *Journal of the American College of Surgeons*, vol. 217, no. 3, pp. 533–555, 2013.
- [2] NC3RS, "National Centre for the Replacement Refinement & Reduction of Animals in Research," 2018. [Online]. Available: <https://www.nc3rs.org.uk/>. [Accessed: 12-Nov-2018].
- [3] F. R. A. J. Rose and R. O. C. Oreffo, "Bone tissue engineering: Hope vs hype," *Biochemical and Biophysical Research Communications*, vol. 292, no. 1, pp. 1–7, 2002.
- [4] E. Hoch, G. E. M. Tovar, and K. Borchers, "Bioprinting of artificial blood vessels: Current approaches towards a demanding goal," *European Journal of Cardio-thoracic Surgery*, vol. 46, no. 5, pp. 767–778, 2014.
- [5] R. Y. Kannan, H. J. Salacinski, K. Sales, P. Butler, and A. M. Seifalian, "The roles of tissue engineering and vascularisation in the development of micro-vascular

- networks: A review," *Biomaterials*, vol. 26, no. 14, pp. 1857–1875, 2005.
- [6] C. W. Patrick Jr, "Adipose Tissue Engineering: The Future of Breast and Soft Tissue Reconstruction Following Tumor Resection," *Seminars in Surgical Oncology*, no. 713, pp. 302–311, 2000.
- [7] R. J. Zdrahala, "Small caliber vascular grafts. Part II: Polyurethanes revisited," *Journal of Biomaterials Applications*, vol. 11, no. 1, pp. 37–61, 1996.
- [8] F. P. W. Melchels, M. A. N. Domingos, T. J. Klein, J. Malda, P. J. Bartolo, and D. W. Hutmacher, "Additive manufacturing of tissues and organs," *Progress in Polymer Science*, vol. 37, no. 8, pp. 1079–1104, 2012.
- [9] W. L. Ng, J. M. Lee, W. Y. Yeong, and M. Win Naing, "Microvalve-based bioprinting-process, bio-inks and applications," *Biomaterials Science*, vol. 5, no. 4, pp. 632–647, 2017.
- [10] D. B. Kolesky, R. L. Truby, A. S. Gladman, T. A. Busbee, K. A. Homan, and J. A. Lewis, "3D bioprinting of vascularized, heterogeneous cell-laden tissue constructs," *Advanced Materials*, vol. 26, no. 19, pp. 3124–3130, 2014.
- [11] C. Kucukgul, B. Ozler, H. E. Karakas, D. Gozuacik, and B. Koc, "3D hybrid bioprinting of macrovascular structures," *Procedia Engineering*, vol. 59, pp. 183–192, 2013.
- [12] J. S. Miller *et al.*, "Rapid casting of patterned vascular networks for perfusable engineered three-dimensional tissues," *Nature Materials*, vol. 11, no. 9, pp. 768–774, 2012.
- [13] W. Wu, A. Deconinck, and J. A. Lewis, "Omnidirectional printing of 3D microvascular networks," *Advanced Materials*, vol. 23, no. 24, pp. 178–183, 2011.

- [14] T. J. Hinton *et al.*, "Three-dimensional printing of complex biological structures by freeform reversible embedding of suspended hydrogels," *Science Advances*, vol. 1, no. 9, p. e1500758, Oct. 2015.
- [15] X. Han *et al.*, "Optimized vascular network by stereolithography for tissue engineered skin," *International Journal of Bioprinting*, vol. 4, no. 2, pp. 1–17, 2018.
- [16] G. S. Kassab, C. A. Rider, N. J. Tang, and Y. C. Fung, "Morphometry of pig coronary arterial trees," *American Journal of Physiology-Heart and Circulatory Physiology*, vol. 265, no. 1, pp. H350–H365, Jul. 1993.
- [17] J. Ravensbergen, J. K. B. Krijger, B. Hillen, and H. W. Hoogstraten, "Merging flows in an arterial confluence: The vertebro-basilar junction," *Journal of Fluid Mechanics*, vol. 304, pp. 119–141, 1995.
- [18] J. Ravensbergen, J. K. B. Krijger, B. Hillen, and H. W. Hoogstraten, "The influence of the angle of confluence on the flow in a vertebro-basilar junction model," *Journal of Biomechanics*, vol. 29, no. 3, pp. 281–299, 1997.
- [19] U. Köhler, I. Marshall, M. B. Robertson, Q. Long, X. Y. Xu, and P. R. Hoskins, "MRI measurement of wall shear stress vectors in bifurcation models and comparison with CFD predictions," *Journal of Magnetic Resonance Imaging*, vol. 14, no. 5, pp. 563–573, Nov. 2001.
- [20] I. Marshall, S. Zhao, P. Papathanasopoulou, P. Hoskins, and X. Y. Xu, "MRI and CFD studies of pulsatile flow in healthy and stenosed carotid bifurcation models," *Journal of Biomechanics*, vol. 37, no. 5, pp. 679–687, 2004.
- [21] D. Arteries, "Vascular Tissue Engineering," pp. 1115–1117, 1999.

- [22] G. Liu, J. Wu, D. N. Ghista, W. Huang, and K. K. L. Wong, "Hemodynamic characterization of transient blood flow in right coronary arteries with varying curvature and side-branch bifurcation angles," *Computers in Biology and Medicine*, vol. 64, pp. 117–126, 2015.
- [23] Morton H. Friedman; Owen J. Deters; Frank F. Mark; C. Brent Barger; Grover M. Hutchins, "Arterial geometry affects hemodynamics. A potential risk factor for atherosclerosis," *Atherosclerosis*, vol. 46, no. 2, pp. 225–231, 1983.
- [24] C. Peng, X. Wang, Z. Xian, X. Liu, and W. Huang, "The Impact of the Geometric Characteristics on the Hemodynamics in the Stenotic Coronary Artery," *PLoS ONE*, vol. 11, no. 6, pp. 1–18, 2016.
- [25] G. Coppola and C. Caro, "Arterial geometry , flow pattern , wall shear and mass transport : potential physiological significance," *Journal of the Royal Society Interface*, no. November 2008, pp. 519–528, 2009.
- [26] C. G. Caro, "Discovery of the Role of Wall Shear in Atherosclerosis," *Arterioscler Thromb Vasc Biol.*, pp. 158–161, 2009.
- [27] Q. Long, X. Y. Xu, M. Bourne, and T. M. Griffith, "Numerical study of blood flow in an anatomically realistic aorto-iliac bifurcation generated from MRI data," *Magnetic Resonance in Medicine*, vol. 43, no. 4, pp. 565–576, 2000.
- [28] H. Meng *et al.*, "Complex hemodynamics at the apex of an arterial bifurcation induces vascular remodeling resembling cerebral aneurysm initiation," *Stroke*, vol. 38, no. 6, pp. 1924–1931, 2007.
- [29] C. D. Murray, "The Physiological Principle of Minimum Work: I. The Vascular System

- and the Cost of Blood Volume.," *Proceedings of the National Academy of Sciences of the United States of America*, vol. 12, no. 3, pp. 207–14, Mar. 1926.
- [30] C. D. Murray, "The Physiological Principle of Minimum Work: II. Oxygen Exchange in Capillaries.," *Proceedings of the National Academy of Sciences of the United States of America*, vol. 12, no. 5, pp. 299–304, 1926.
- [31] M. Zamir, "Optimality principles in arterial branching," *Journal of Theoretical Biology*, vol. 62, no. 1, pp. 227–251, Oct. 1976.
- [32] X. Han, R. Bibb, and R. Harris, "Design of bifurcation junctions in artificial vascular vessels additively manufactured for skin tissue engineering," *Journal of Visual Languages and Computing*, vol. 28, pp. 238–249, 2015.
- [33] J. Bloomenthal, "Skeletal design of natural forms," University of Calgary, Canada, 1995.
- [34] J. Kretschmer, C. Godenschwager, B. Preim, and M. Stamminger, "Interactive patient-specific vascular modeling with sweep surfaces," *IEEE Transactions on Visualization and Computer Graphics*, vol. 19, no. 12, pp. 2828–2837, 2013.
- [35] Y. Zhang, Y. Bazilevs, S. Goswami, C. L. Bajaj, and T. J. R. Hughes, "Patient-specific vascular NURBS modeling for isogeometric analysis of blood flow," *Proceedings of the 15th International Meshing Roundtable, IMR 2006*, vol. 196, pp. 73–92, 2006.
- [36] O. Gourmel *et al.*, "A gradient-based implicit blend," *ACM Transactions on Graphics*, vol. 32, no. 2, pp. 1–12, Apr. 2013.
- [37] R. Krasauskas, "Branching blend of natural quadrics based on surfaces with rational offsets," *Computer Aided Geometric Design*, vol. 25, no. 4–5, pp. 332–341, 2008.

- [38] Y. Cai, X. Ye, C. Chui, and J. H. Anderson, "Constructive algorithms of vascular network modeling for training of minimally invasive catheterization procedure," *Advances in Engineering Software*, vol. 34, no. 7, pp. 439–450, 2003.
- [39] X. Ye, Y. Y. Cai, C. Chui, and J. H. Anderson, "Constructive modeling of G1 bifurcation," *Computer Aided Geometric Design*, vol. 19, no. 7, pp. 513–531, 2002.
- [40] X. Han, R. Bibb, and R. Harris, "Engineering design of artificial vascular junctions for 3D printing," *Biofabrication*, vol. 8, no. 2, pp. 1–13, 2016.
- [41] T. Papaioannou and Stefanadis C, "Vascular Wall Shear Stress : Basic Principles and," *Hellenic Journal of Cardiology*, vol. 46, no. January 2005, pp. 9–15, 2014.
- [42] J. Khamassi, C. Bierwisch, and P. Pelz, "Geometry optimization of branchings in vascular networks," *Physical Review E*, vol. 93, no. 6, p. 062408, Jun. 2016.
- [43] I. Gibson, D. W. Rosen, and B. Stucker, "Extrusion-Based Systems," in *Additive Manufacturing Technologies*, Boston, MA: Springer US, 2010, pp. 160–186.
- [44] A. Gebhardt, *Generative Fertigungsverfahren*. München: Carl Hanser Verlag GmbH & Co. KG, 2013.
- [45] S. Maruo and K. Ikuta, "Submicron stereolithography for the production of freely movable mechanisms by using single-photon polymerization," *Sensors and Actuators A: Physical*, vol. 100, no. 1, pp. 70–76, Aug. 2002.
- [46] S. Engelhardt, "3D-Microfabrication of Polymer-Protein Hybrid Structures with a Q-Switched Microlaser," *Journal of Laser Micro/Nanoengineering*, vol. 6, no. 1, pp. 54–58, Mar. 2011.

- [47] S. Engelhardt *et al.*, "Fabrication of 2D protein microstructures and 3D polymer-protein hybrid microstructures by two-photon polymerization," *Biofabrication*, vol. 3, no. 2, 2011.
- [48] Santokh S. Labana, *Chemistry and Properties of Crosslinked Polymers*. New York: Academic Press, 1977.